Photochemical & Photobiological Sciences

Dynamic Article Links

Cite this: *Photochem. Photobiol. Sci.*, 2012, **11**, 1032

www.rsc.org/pps

PAPER

Triplet state of 4-methoxybenzyl alcohol chemisorbed on silica nanoparticles†‡

Valeria B. Arce,[a,b] Sonia G. Bertolotti,[c] Fernando J. V. E. Oliveira,[d] Claudio Airoldi,[e] Antonio Arques,[f] Lucas Santos-Juanes,[f] Mónica C. Gonzalez,[a] Carlos J. Cobos,[a] Patricia E. Allegretti[b] and Daniel O. Mártire*[a]

Received 9th November 2011, Accepted 9th February 2012
DOI: 10.1039/c2pp05370e

The knowledge of photochemical kinetics in colloidal systems is important in understanding environmental photochemistry on dispersed solid surfaces. As model materials for the chemically sorbed organic compounds present in natural environments, modified silica nanoparticles (NPs) were obtained here by condensation of the silanol groups of fumed silica nanoparticles with 4-methoxybenzyl alcohol. These particles were characterized by different techniques. To evaluate their toxicity, the inhibition of the natural luminescence emission of the marine bacterium *Vibrio fischeri* in suspensions of the particles was measured. Laser flash-photolysis experiments (λ_{exc} = 266 nm) performed with NP suspensions in acetonitrile–aqueous phosphate buffer mixtures showed the formation of the lowest triplet excited state of the chemisorbed organic groups (λ_{max} = 390 nm). DFT calculations of the absorption spectrum of this radical support the assignment. From the calculated triplet energy, a thermodynamically favorable energy transfer from these triplet states to oxygen to yield singlet molecular oxygen is predicted. A value of 0.09 was measured for the quantum yield of singlet molecular oxygen generation by air-saturated suspensions of the nanoparticles in the mixture of solvents acetonitrile–aqueous phosphate buffer. The quantum yield of singlet molecular oxygen generation by the free 4-methoxybenzyl alcohol in the same solvent is 0.31.

1. Introduction

Organic–inorganic hybrid materials based on nanosized inorganic particles are an emerging field because of their importance in diverse applications in electronics, optics, engineering, and chemical sensing. The well-established silica chemistry facilitates the modification of silica-based nanoparticles to obtain the hybrid materials.

The knowledge of photochemical kinetics in colloidal systems is important in understanding environmental photochemistry on dispersed solid surfaces. While fumed silica has been used as a support for studying photophysics at gas–solid interfaces, few studies of photophysics at solution–dispersed particle interfaces have appeared in the literature.[1–4]

We employ here a procedure based on reaction (1), which is a modification of the condensation method reported in the literature[3–6] to prepare derivatized fumed silica nanoparticles as model materials for the chemically sorbed organic compounds present in natural environments. Since we are interested in evaluating the effect of alcohol adsorption on the surface, we determined the surface area,[7] and the number of modified silanols.[2,3,8] The characterization also includes toxicity assays performed with suspensions of the particles. These measurements appear sufficient to evaluate both the biocidal effects of these hybrid materials on microorganisms and their secondary effects when contained in surface and drinking water.

Laser flash-photolysis experiments (λ_{exc} = 266 nm) performed with suspensions of the nanoparticles in acetonitrile–aqueous phosphate buffer mixtures showed the formation of transient species. Theoretical calculations of absorption spectra of radicals and excited states were used to support the assignment of the detected transient species. Moreover, the ability of the organic groups chemically sorbed on the particles to generate and quench singlet molecular oxygen, $O_2(^1\Delta_g)$, was also evaluated.

[a]*Instituto de Investigaciones Fisicoquímicas Teóricas y Aplicadas (INIFTA), Universidad Nacional de La Plata, Casilla de Correo 16, Sucursal 4, (1900) La Plata, Argentina. E-mail: dmartire@inifta.unlp.edu.ar; Fax: +154221 4254642; Tel: +54 221 4257430/7291*
[b]*LADECOR, Departamento de Química, Facultad de Ciencias Exactas, Universidad Nacional de, (1900) La Plata, Argentina*
[c]*Departamento de Química, Universidad Nacional de Río Cuarto, (5800) Río Cuarto, Argentina*
[d]*Departamento de Química, CCEN, Universidade Federal da Paraíba (UFPB), 58059-900 João Pessoa, Paraíba, Brazil*
[e]*Chemistry Institute, University of Campinas, P.O. Box 6154, 13084-971 Campinas, São Paulo, Brazil*
[f]*Grupo de Procesos de Oxidación Avanzada, Dpto de Ingeniería Textil y Papelera, Campus de Alcoy de la Universidad Politécnica de Valencia, 03801 Alcoy, Spain*

† Dedicated to Prof. Kurt Schaffner on the occasion of his 80th birthday.

‡ Electronic supplementary information (ESI) available: TEM images, ^{29}Si NMR in solid state of the modified nanoparticles. Percentage of luminescence inhibition *vs*. the concentration of benzyl alcohol. FTIR spectra of 4-methoxybenzyl alcohol experimental and simulated. Experimental IR wavenumbers for NP and 4-methoxybenzyl alcohol. See DOI: 10.1039/c2pp05370e

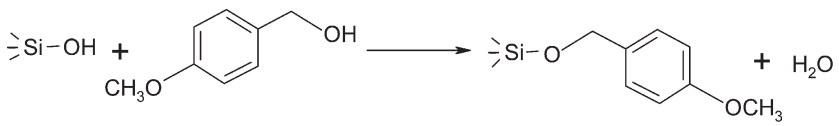

(1)

2. Experimental

2.1 Materials

Fumed silica (Sigma, specific surface area; SSA = 390 ± 40 m^2 g^{-1}, particle diameter estimated from the SSA = 7 nm) was dried in a crucible for 15 h at 120 °C and then in a muffle for 3 h at 250 °C and stored in a desiccator. The chemicals *o*-xylene and 4-methoxybenzyl alcohol (Aldrich) were distilled onto molecular sieves, which had been dried at 250 °C for 4 h. Ethyl acetate (Ciccarelli, p.a.), CaH_2 (Fluka), $CaCl_2$ (Sigma-Aldrich), and K_2HPO_4, and KH_2PO_4 (Merck) were used without further purification.

Perinaphthenone-2-sulphonic acid (1*H*-phenalen-1-one-2-sulphonic acid, PNS) was synthesized as described by Nonell *et al.*[9] Distilled water (>18 MΩ cm, <20 ppb of organic carbon) was obtained from a Millipore (Bedford, MA) system.

2.2 Synthesis of the nanoparticles

For the synthesis of the particles modified with 4-methoxybenzyl alcohol (NP), 90 mL of this alcohol and 140 mL of *o*-xylene were added to 3.0 g of silica nanoparticles. The mixtures were placed in a Soxhlet extractor containing CaH_2 equipped with a condenser with anhydrous $CaCl_2$, and refluxed for 24 h. The products were filtered with 20 nm nylon filters, washed with 50 mL hot *o*-xylene and finally with 50 mL ethyl acetate. The resulting gel was first dried at 0.1 Torr and at room temperature for 3 h and then at 120 °C for 5 h. White powders were obtained.

The silica nanoparticles modified with *n*-butanol and benzyl alcohol used for comparison purposes were synthesized and characterized as described elsewhere.[3,8]

Acetonitrile or 1 : 1 mixtures of acetonitrile–aqueous phosphate buffer (pH = 6.4) were used as the solvents for the time-resolved experiments.

2.3 Fourier transform infrared spectroscopy (FTIR)

Fourier transform infrared (FTIR) spectra were recorded on a Bruker EQUINOX 55 instrument, using KBr disks. For each spectrum, 128 scans in the range 4000–400 cm^{-1} were recorded. The resolution was 2 cm^{-1}.

2.4 Brunauer–Emmett–Teller (BET) analysis

The specific surface area (SSA) was determined *via* nitrogen (N_2) adsorption isotherms at 77 K in the reduced pressure range from 0.04 to 0.12 using the Brunauer–Emmett–Teller (BET) method.[10] For this purpose a gas adsorption apparatus (Micromeritics ASAP 2020 V1.04 E) was employed.

2.5 ^{13}C and ^{29}Si nuclear magnetic resonance (NMR)

Nuclear magnetic resonance spectra were obtained with a Bruker Avance II 400 spectrometer at room temperature, by assaying approximately one gram of the solid sample compacted into a 7 mm zirconium oxide rotor. The measurements were performed at 75.47 and 59.61 MHz for carbon and silicon, with a magic angle spinning (MAS) technique at 10 kHz. To increase the signal to noise ratio, the cross-polarization (CP) technique was applied. NMR spectra of ^{13}C and ^{29}Si were obtained with pulse repetition of 1 and 3 s and contact times of 1 and 3 ms, respectively.

2.6 Thermogravimetry (TG)

The thermogravimetric analysis was performed with a Shimadzu TGA-50 unit at a heating rate of 5 °C min^{-1} and nitrogen flow of 50 mL min^{-1}. The instrument was calibrated with $CaC_2O_4 \cdot H_2O$.

2.7 Total organic carbon (TOC)

TOC was measured with a high-temperature carbon analyzer (Shimadzu TOC 5000 A) using a calibration curve with potassium biphthalate standard. Standard solutions were run before each analysis to check for instrumental shifts. To obtain the TOC content, 10.0 mg of the NPs was dissolved in 1 mL 48.5% w/w HF and water was added to this solution to obtain a final volume of 10.00 mL.

2.8 Transmission electron microscopy

The transmission electron microscopy (TEM) images were obtained in a Philips CM 200 equipped with an ultratwin objective lens and acceleration voltage of 200 kV. The results obtained from SiO_2 or NP suspensions (see TEM images of NP in Fig. S1 of the ESI‡) yielded aggregated nanoparticles of individual average diameters of 7 nm, in agreement with the data provided by the supplier of the bare silica particles.

2.9 *Vibrio fischeri* luminescence assays

Although a wide range of biological assays are available for the evaluation of toxicity, the inhibition of the natural luminescence emission of the marine bacterium *Vibrio fischeri* has been chosen.[11] This method is widely used because of its convenience and high sensitivity, when compared to activated sludge-based respirometric methods, which are more suitable to study the applicability of a biological process on an effluent.[12,13]

Luminescent assays were carried out according to the standardized ISO 11348-3 norm, using lyophilised bacteria (*Vibrio fischeri*, NRRL B-11177). The standard procedure was employed for reconstitution of the bacteria, using a salty solution obtained from Macherey-Nagel. The luminescence was measured by a Luminometer Lumifix-Bio-10, also supplied by Macherey-Nagel. Toxicity was determined after 15 min incubation. Distilled water and zinc sulfate were used in control experiments. All samples were neutralized before analysis.

2.10 Laser flash-photolysis (LFP) experiments

LFP experiments were performed by excitation with the fourth harmonic of a Nd:YAG (Spectron SL 400) laser (18 ns FWHM). The analysis light from a 150 W Xe arc lamp was passed through a PTI monochromator and detected by a R666 Hamamatsu photomultiplier coupled to a HP54504 digital oscilloscope.

2.11 Experiments for the determination of the $O_2(^1\Delta_g)$ quantum yield, Φ_Δ

Laser irradiation of the sensitizer PNS at 355 nm with *ca.* 18 ns pulse width was carried out with a Nd:YAG laser (Spectron Laser SL400). After the laser pulse, the phosphorescent emission from singlet oxygen was registered at 1270 nm with a Ge amplified detector (Judson J16/8Sp). The emission previously passed through cut-off (<1000 nm) and interference (1270 nm) filters. The output of the detector was coupled to a digital oscilloscope and to a personal computer for the signal processing. The signals from 10 laser pulses were averaged and the obtained trace was fitted to a monoexponential function of time, characterized by τ_Δ, the singlet oxygen lifetime. The detection and acquisition systems are described elsewhere.[14]

2.12 Quenching of $O_2(^1\Delta_g)$ experiments

Rose Bengal (A^{532} = 0.50–0.55) was used as the sensitizer in all the $O_2(^1\Delta_g)$ quenching experiments. To measure the sum of the rate constants of the physical quenching and chemical reaction channels, k_t, for the deactivation of $O_2(^1\Delta_g)$ by the 4-methoxybenzyl alcohol and the NP in acetonitrile, the excitation source was the second harmonic of a Nd:YAG Litron laser.[15] The luminescence was measured as already described.[16]

2.13 Computational details

The geometrical structures of the singlet ground states and the lowest lying triplet excited states of the 4-methoxybenzyl alcohol and the cluster were optimized using the hybrid B98[17] method of the density functional theory, DFT, without symmetry constraints. In all cases the 6-311++G(d,p) basis set was employed. The DFT calculations were associated with the conductor-like polarizable continuum model, CPCM,[18] with a dielectric constant for acetonitrile of 35.688. In this way, the broadening of the absorption bands due to bulk solvent effects was taken into account. In all cases, real harmonic vibrational frequencies were obtained, assuring that computed structures correspond to a minimum on the potential energy surface. Electronic energies and oscillator strengths for a number of transitions were calculated by using the time dependent density functional theory, TD-DFT, at the mentioned levels of theory. The oscillator strength depends on electronic, Frank–Condon and spin factors, which reduces the unity maximum value expected for a totally allowed transition and provides information on the intensity of the absorption band. To compare with the experimental results, the theoretical bands were approached with individual Gaussian functions characterized with full width values σ (at the $1/e$ height of the bands) and summed over all relevant electronic transitions.[19] For the present systems, σ values of 2000 cm^{-1} were found appropriate to reproduce the experimental absorption bands. As a measure of the spin contamination, the obtained expectation values of the <S2> operator were not greater than 2.04, close to the exact value of 2.00 for triplet states. All the calculations were performed with the Gaussian 03 software package.[20]

3. Results and discussion

3.1 Characterization of the nanoparticles

NMR spectra for silicon and carbon nuclei in solid state provide important features related to silica nanoparticles. Three typical ^{29}Si signals were observed (see ESI, Fig. S2‡), referring to silica network, being assigned to $Si(OSi)_4$, Q^4, $Si(OSi)_3OH$, Q^3 and $Si(OSi)_2(OH)_2$, Q^2 chemical species at −110, −99 and −95 ppm,[21,22] respectively. Although low signal-to-noise ratio is observed, it is possible to detect the typical species from the silica framework due to silanol and siloxane bonding. For the NP sample (Fig. 1), six distinct ^{13}C NMR signals were observed, as expected from the structure. The spectrum shows the signals of the aromatic ring carbon atoms 3 and 4 located in different chemical environments at 129 and 112 ppm, respectively. The signals at 65 and 132 ppm (1 and 2) refer to the carbon bond to the O–Si≡ moiety and that from the benzene ring, respectively. Finally, the peak at 159 ppm (5) is assigned to the aromatic carbon atom bonded to the methoxy group (6) observed at 53 ppm. Both spectra are in total agreement with the expected derivatization of the silica particles with the alcohol. Spectral simulations performed with ChemDraw Ultra 8.0, Cambridge Software, confirm the present attributions.

The values of SSA of the NPs are shown in Table 1. Modification of the silica nanoparticles results in a decrease in surface area, ΔSSA,[23] with respect to the value of 390 ± 40 $m^2\ g^{-1}$, corresponding to the bare SiO_2 nanoparticles. The decrease in SSA upon silica modification with organic compounds was reported for different systems.[24–27] This behavior can be explained based on the preferential adsorption of the nitrogen molecules on the silanol groups. By assuming that there is no nitrogen adsorption on the modified silanols, it is possible to obtain the fraction of derivatized silanol groups, *f*(SiOR), from the SSA data (Table 1).

The mass of one bare SiO_2 nanoparticle (3.95×10^{-19} g) is calculated from the average volume of the nanoparticle and the density of silica (2200 kg m^{-3}).[28] The average number of silanol groups in one nanoparticle of bare SiO_2 was estimated to be 708 by assuming spherical particle of radius r = 3.5 nm and 4.9 OH

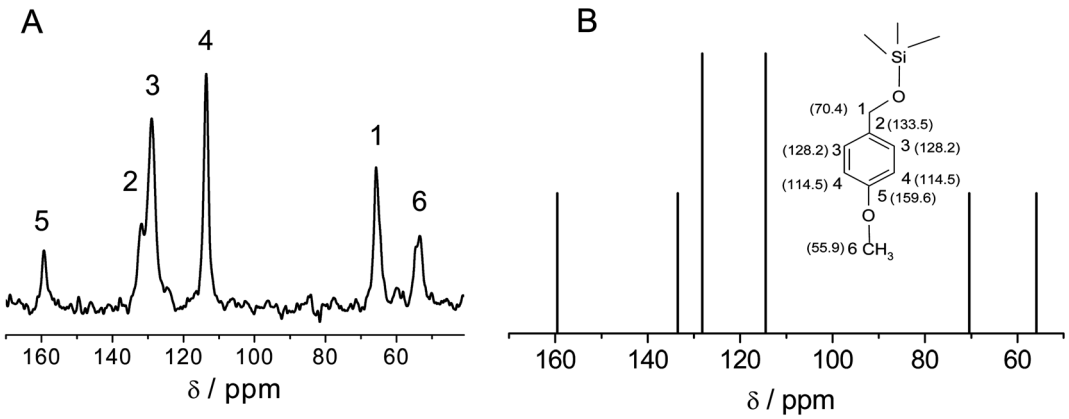

Fig. 1 A: ^{13}C NMR solid state spectra for NP. B: Simulated spectrum with ChemDraw 8.0 and signal assignment.

Table 1 Specific surface area (SSA), decrease of SSA with respect to the bare SiO_2 nanoparticles (ΔSSA), fraction of modified silanol groups, *f*(SiOR), and percentage of organic compounds in mass (%OG)

Parameter	Value
SSA ($m^2\ g^{-1}$)	191 ± 2
ΔSSA ($m^2\ g^{-1}$)[a]	199 ± 40
f(SiOR)[a,b]	0.51 ± 0.18
%OG (w/w)[c]	9 ± 1
%OG (w/w)[a,d]	15 ± 6
%OG (w/w)[e]	16

[a] Error bars calculated from the propagation of the error bars in SSA. [b] Calculated as ΔSSA/390 $m^2\ g^{-1}$. 390 $m^2\ g^{-1}$ is the value of SSA for the bare silica nanoparticles. [c] From the TG experiments. [d] From SSA. [e] From TOC measurements.

groups nm^{-2}.[29] From these data and *f*(SiOR), the %OG is calculated (Table 1).

The %OG bonded to silica was also calculated from the mass loss of the samples in the TG experiments from 200 to 700 °C.[30] The calculation yields a value of 9 ± 1% for %OG of NP (Table 1). In general, there is a very good agreement between the data obtained from the three independent experiments. However, the %OG obtained from TG and SSA are more reliable because higher values of %OG can be obtained from TOC measurements due to CO_2(g) adsorption generated during the acidification of the samples performed previous to the TOC measurement.[31,32]

The FTIR spectrum of NP shows peaks at 2849, 2924, 2961, 3014 and 1517 cm^{-1} (see ESI, Table S1‡), which are not observed for bare silica nanoparticles (Fig. 2). The additional peaks are also present in the spectra of 4-methoxybenzyl alcohol (see ESI, Fig. S4‡). As can be seen in Fig. S4,‡ there is a very good agreement between experimental and calculated (see below) IR spectra, except for the peak centered at around 3500 cm^{-1}, assigned to H-bonding[33] not considered in the DFT calculation. The ratio of the intensity of the bands due to Si–OH absorption at 3400–3450 cm^{-1} and those assigned to Si–O–Si at 1100 cm^{-1} is smaller for the derivatized silica particles than for the bare ones. Therefore, a considerable diminution of the amount of silanol groups occurs after modification, as expected from the covalent bonding between the nanoparticles and the organic molecules (reaction (1)). Any IR absorption due to the vibration modes assigned to Si–O–C bonds[34] is masked by the strong Si–O–Si absorption signals at 1100 cm^{-1}.

3.2 Toxicity assays

According to García *et al.*[35] germination (phytotoxicity) tests are not adequate for determining toxicity of nanoparticles. On the contrary, *Daphnia magna* and *Vibrio fischeri* tests provide more reliable and reproducible information about the toxicity of nanoparticles.

Comparative *Vibrio fischeri* toxicity experiments with nanoparticles modified with *n*-butanol and benzyl alcohol were performed. These samples were prepared by employing the method reported elsewhere.[3,8] The percentages of organic groups (%OG) determined for the nanoparticles modified with *n*-butanol and benzyl alcohol from the values of SSA of these samples were 6 ± 3 and 10 ± 3, respectively.

Vibrio fischeri assays with bare SiO_2 nanoparticles or with the particles modified with *n*-butanol showed no toxicity for suspensions of concentrations up to 1.0 g L^{-1} (results not shown).

The undetectable toxicity for the 1.0 g L^{-1} suspensions of the particles modified with *n*-butanol indicates that under the experimental conditions the toxicity of the butyl ether groups bonded to the nanoparticles is also negligible. From the value of %OG shown in Table 1, it can be estimated that the concentration of the butyl groups in a 0.45 g L^{-1} suspension of the particles modified with *n*-butanol is about 0.03 g L^{-1}.

The toxicity of a chemical substance is characterized by the value of EC_{50}, the concentration of the compound that produces an inhibition of bioluminescence of 50% compared to a blank assay. The undetectable toxicity of the organic groups at a concentration of 0.03 g L^{-1} is in line with the reported value of $EC_{50} \approx 3$ g L^{-1} for free *n*-butanol.[36]

Fig. S3 in the ESI‡ shows the measured *E*%, percentage of luminescence inhibition *vs.* the concentration of benzyl alcohol. The linear plots of log *C vs.* log[*E*%/(100−*E*%)] (not shown) yielded EC_{50} = (0.45 ± 0.01) g L^{-1} and EC_{50} = (0.31 ± 0.09) g L^{-1} for benzyl alcohol and 4-methoxybenzyl alcohol, respectively.

Experiments performed with 1 g L^{-1} suspensions of the particles modified with benzyl alcohol show a luminescence inhibition of about 30%. This result compared to the undetectable

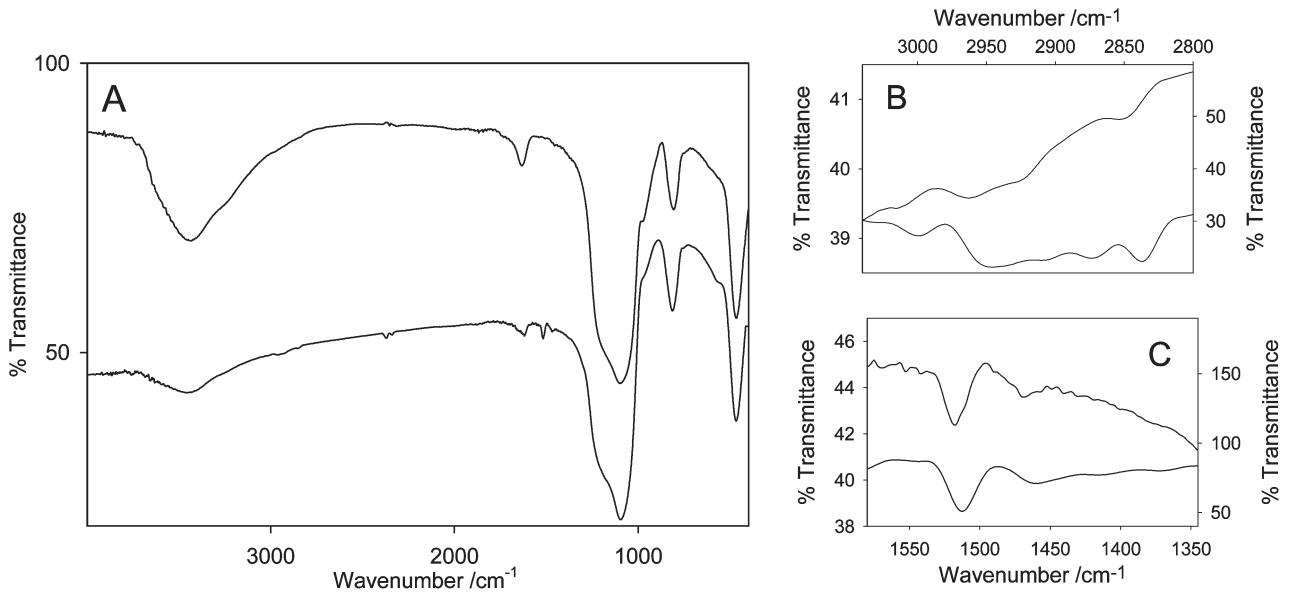

Fig. 2 A: FTIR spectra of: activated bare silica (upper trace), and NP (lower trace). B, C: Expanded FTIR spectrum of: NP (upper trace) and 4-methoxybenzyl alcohol (lower trace).

toxicity found for the naked silica nanoparticles is indicative of the presence of some toxicity due to the attached organic groups.

From the concentration of the particles modified with benzyl alcohol (1 g L^{-1}) and the 10% of %OG in mass, a concentration of 0.1 g L^{-1} organic matter in the suspension is obtained. For this concentration of free alcohol an inhibition effect of about 9% was measured in experiments in the absence of nanoparticles (Fig. S3‡). This value is lower than the 30% inhibition observed for the 1 g L^{-1} suspensions of the particles modified with benzyl alcohol.

Vibrio fischeri experiments with 1 g L^{-1} of the particles derivatized with 4-methoxybenzyl alcohol (with the same fraction of derivatized silanols as those modified with benzyl alcohol) yielded a value of $E\% = 61\%$. This result shows the higher toxicity of the particles derivatized with 4-methoxybenzyl alcohol compared to those modified with the benzyl alcohol. From the NP concentration (1 g L^{-1}) and the 20% of %OG in mass (Table 1), a concentration of 0.2 g L^{-1} organic matter in the suspension is obtained. For this concentration of free alcohol an inhibition effect of about 48% was measured in experiments in the absence of nanoparticles (results not shown). This value is lower than the 61% inhibition observed for the 1 g L^{-1} NP.

When comparing the toxicity of the particles suspensions to that of solutions containing the same concentration of organic groups, we should keep in mind that the toxicity of the nanoparticles is related to surface composition, which determines the nature of the contact of the particle with living matter. The physical and chemical properties of the surface control the ability of the particles to adsorb biomolecules, to disrupt cell membranes, and to adhere to a given substrate. The chemical composition of a surface will thus ultimately determine the toxicity of a given kind of nanomaterial.[37]

The higher toxicity of the alcohol bonded to particles could be caused by the favored bacterial adhesion to the hydrophobized surfaces, which present higher bacterial sticking coefficients and stronger adhesion forces than bare silica surfaces.[38] As a result, the local concentration of organic groups in contact with the bacteria is higher than in solution. The results obtained here show that the toxicity of the particles modified with the alcohols correlates with that of the solutions of the alcohols, *i.e.*, butanol < benzyl alcohol < 4-methoxybenzyl alcohol.

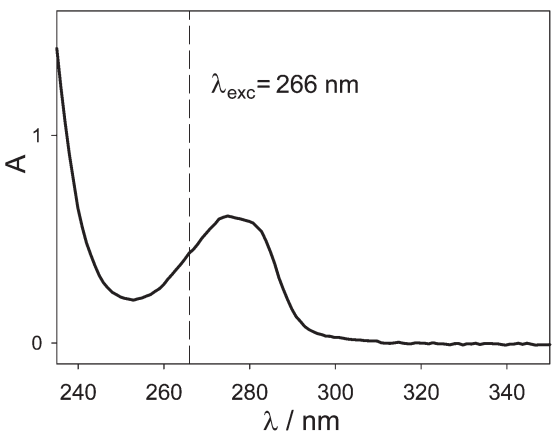

Fig. 3 UV-visible absorption spectrum of a 0.6 g L^{-1} suspension of NP in 1 : 1 acetonitrile–aqueous phosphate buffer. The excitation wavelength of 266 nm employed in the photochemical experiments is also shown. The scattering component of the NP samples was subtracted according to Ruiz *et al.*[3]

3.3 Photochemical experiments

The UV-visible absorption spectrum of a suspension of the nanoparticles in 1 : 1 acetonitrile–aqueous phosphate buffer is shown in Fig. 3.

Laser flash-photolysis (LFP) experiments performed with 0.8 g L^{-1} dispersions of NP in Ar-saturated 1 : 1 acetonitrile–

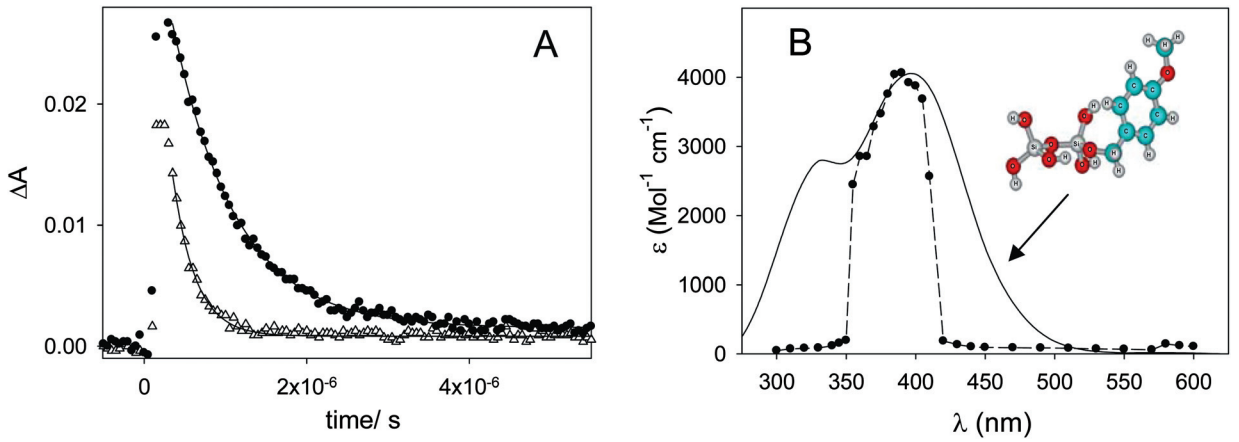

Fig. 4 A: Traces obtained at 380 nm with the suspensions employed in the main figure under: Ar-saturation (●); and air-saturation (Δ). The solid lines show the fitting to single exponential decay functions. B: Absorption spectrum of the transient species obtained from LFP experiments (λ_{exc} = 266 nm) performed with Ar-saturated solutions of 4-methoxybenzyl alcohol in acetonitrile–aqueous phosphate buffer (●). The solid line shows the T–T absorption coefficients calculated for the cluster. The experimental spectrum is normalized to the calculated one.

aqueous phosphate buffer showed formation of a transient species with maximum at around 390 nm (see absorption spectrum in Fig. 4).

The transient species could be formed upon photoionization of the organic moiety to yield a radical cation. However, assuming an ionization potential of the organic moiety similar to that of the 4-methoxybenzyl alcohol (771 kJ mol^{-1}),[39] we conclude that the photoionization cannot take place in a 266 nm monophotonic process. Since the low laser fluence employed in the experiments guarantees that the transient species are formed in a monophotonic event, formation of the cation radicals is neglected. This is in line with the absence of absorption detected in the region where the solvated electron (λ_{max} = 720 nm)[40] and the radical cation of the 4-methoxybenzyl alcohol (λ_{max} = 290 and 450 nm[41]) absorb.

The photolysis of NP at 266 nm could lead to the Si–O–C scission according to reaction (2).

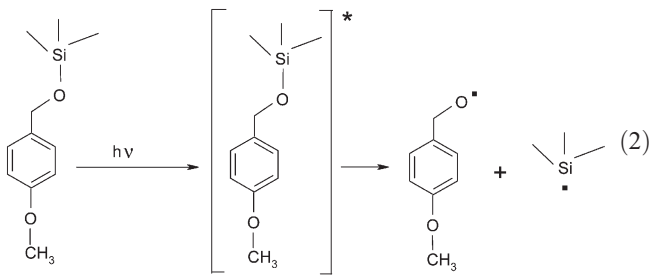

However, the (4-methoxybenzyl)oxyl radical formed as a product of reaction (2) was reported to absorb in the visible region with a maximum at 560 nm.[42] Moreover, from TD-DFT calculations it was possible to obtain the UV-visible spectrum of the radical, which also shows absorption in the visible region. The absorption maximum calculated at the B98/6-311++G(d,p) level of theory for the solvent acetonitrile is located at 533 nm. The energy difference between the experimental absorption maximum, 2.19 eV,[42] and that calculated here, 2.33 eV, is 0.11 eV. This value is much smaller than the mean unsigned error in the electronic excitation energy reported for the B98 method of 0.57 eV.[43] Thus, the transient species observed here cannot be assigned to the (4-methoxybenzyl)oxyl radical.

A reaction route leading to the formation of silica chemisorbed benzyl radicals can also be neglected here because these radicals show an absorption maximum at 320 nm.[8] The 4-methoxybenzyl radical also shows an absorption maximum at 320 nm in solution.[44]

The decay rate of the transient measured here at 380 nm increases with increasing O_2 concentration. The oxygen-dependent decay (Fig. 4A) suggests that the observed transient species may be a chemisorbed triplet state. From the oxygen solubility data in acetonitrile and water,[45,46] it is possible to estimate an oxygen concentration of 0.5 mM in the air-saturated solvent mixture employed here to suspend the particles. From these data and the transient decays observed in Ar- (1.3×10^6 s^{-1}) and air-saturated samples (3.6×10^6 s^{-1}), a bimolecular rate constant of 4.9×10^9 M^{-1} s^{-1} is obtained. Should the transient species be a triplet state, then the spin statistical factor for the energy transfer from this species to oxygen is 1/9,[47] and a value of 4.4×10^{10} M^{-1} s^{-1} is obtained for the diffusion-controlled rate constant of the particles with molecular oxygen, in complete agreement with that calculated for nanoparticles of the same size in the same medium ($k_{diff} \geq 3 \times 10^{10}$ M^{-1} s^{-1}).[3] This result is an evidence for the quenching of the triplet states by dissolved molecular oxygen.

The absorption spectrum of the transient species obtained in comparative LFP experiments with Ar-saturated 4-methoxybenzyl alcohol solutions (Fig. 5) is similar to that obtained from LFP experiments performed with the NP suspensions (Fig. 4). The assignment of the free and chemisorbed species to triplet states, which completely decay to the ground state is supported by our inability to detect changes in the UV-visible absorption spectra of N_2-saturated solutions of the alcohol and suspensions of NP upon irradiation (λ_{exc} = 266 nm) during 1 h employing a laser fluence of 12 ± 3 mJ per pulse at a repetition rate of 10 Hz.

According to the LFP and steady-state irradiation results, the assignment of the transient species observed in Fig. 4 and Fig. 5 to chemisorbed and free triplet states, respectively, seems reasonable. To further support this hypothesis, DFT calculations were

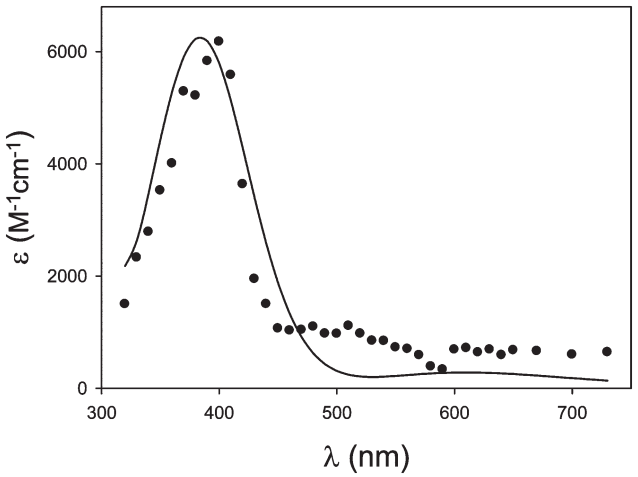

Fig. 5 Absorption spectrum of the transient species obtained from LFP experiments (λ_{exc} = 266 nm) performed with Ar-saturated solutions of 4-methoxybenzyl alcohol in acetonitrile–aqueous phosphate buffer (●). The solid line shows the T–T absorption coefficients calculated for the alcohol. The experimental spectrum is normalized to the calculated one.

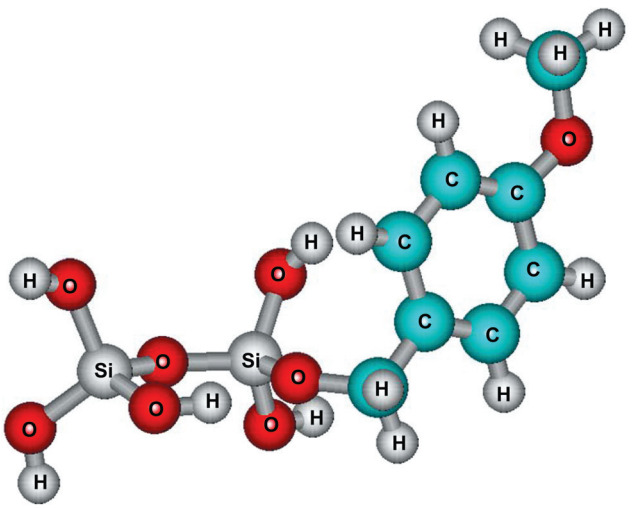

Fig. 6 Molecule employed to model the 4-methoxybenzyl alcohol chemisorbed on the silica nanoparticles (cluster).

performed. The chemisorbed triplet states were modeled with the molecule shown in Fig. 6 which, hereafter, we denote as cluster. As can be seen in Fig. 4 and 5 there is a relatively good agreement between the experimental and calculated T–T absorption spectra for the chemisorbed (modeled with the cluster) and free triplet states. The calculated triplet energies for the alcohol and the cluster are 328.9 and 327.2 kJ mol^{-1}, respectively.

The calculated energies of both chemisorbed and free triplet states are higher than the energy (94.4 kJ mol^{-1})[48] required to promote ground-state oxygen to $O_2(^1\Delta_g)$. To confirm the generation of $O_2(^1\Delta_g)$, time-resolved phosphorescence experiments were performed.

Values of Φ_Δ were obtained using the intensity of the time-resolved 1270 nm singlet oxygen phosphorescence as a probe and the sensitizer PNS as a reference standard (Φ_Δ = 1)[49] (Table 2).

Table 2 Singlet oxygen quantum yield (Φ_Δ) for 4-methoxybenzyl alcohol solutions and NP suspensions

	Φ_Δ in acetonitrile	Φ_Δ in 1 : 1 acetonitrile–aqueous phosphate buffer
4-Methoxybenzyl alcohol	0.47 ± 0.07	0.31 ± 0.06
NP	0.09 ± 0.03	0.09 ± 0.03

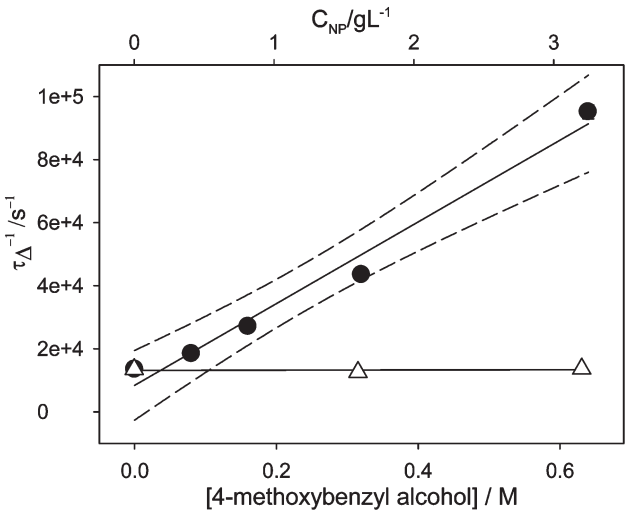

Fig. 7 Plots of τ_Δ^{-1} for the 4-methoxybenzyl alcohol (●) and for the NP (Δ) in acetonitrile.

The method assumes that the flux of absorbed photons is the same in the homogeneous and in micro-heterogeneous media. To guarantee this condition, for the NP the scattering component at the excitation wavelength was subtracted according to Ruiz *et al.*[3]

The time-resolved phosphorescence signals from the air-saturated PNS and 4-methoxybenzyl alcohol solutions and the nanoparticle dispersions showed a single exponential decay both when acetonitrile or 1 : 1 acetonitrile–aqueous phosphate buffer were used as solvents. The measured lifetime of $O_2(^1\Delta_g)$, τ_Δ, in acetonitrile was 68 μs in complete agreement with reported data,[50] whereas in the acetonitrile–aqueous phosphate buffer mixture τ_Δ was 16 μs.

As can be seen in Table 2, lower singlet oxygen quantum yields were obtained for the particles suspensions compared to those of the free alcohol in the same media. There is no apparent reason (*e.g.* electronic interaction) to explain a lower intersystem crossing efficiency for the chemisorbed chromophore compared to that of the free alcohol. Thus, the lower singlet oxygen quantum yields should be related to deactivation of triplet states at the particle's surface, which is in agreement with the faster decay rate of the triplet states (1.3×10^6 s^{-1}, see Fig. 4A) observed in the Ar-saturated suspensions of the NP compared to that detected in the Ar-saturated the solutions of the alcohol (7.3×10^4 s^{-1}, result not shown).

To determine the overall quenching rate constant (k_t) of $O_2(^1\Delta_g)$ by the 4-methoxybenzyl alcohol and by the NP in acetonitrile, the decay of the time-resolved $O_2(^1\Delta_g)$ phosphorescence signal was measured by employing Rose Bengal as the sensitizer (λ_{exc} = 532 nm). The Stern–Volmer plots are shown in Fig. 7.

The slope of the Stern–Volmer plot obtained for the alcohol yields $k_t = (1.3 \pm 0.2) \times 10^5\ M^{-1}\ s^{-1}$. As can be seen in Fig. 7, τ_Δ measured in 0.8–3.2 g L^{-1} dispersions of the NP was independent of the concentration. This observation means that the concentration of surface bonded quencher is too small to affect the lifetime of singlet oxygen within the range of the quencher concentration.

4. Conclusions

Upon irradiation with UV light of the suspensions of silica nanoparticles modified with 4-methoxybenzyl alcohol, transient species are formed. The assignment of these species to chemisorbed triplet states is supported by DFT calculations. The chemisorbed triplet states are quenched by ground state oxygen to yield singlet molecular oxygen with a quantum yield of 0.09.

Acknowledgements

The authors thank Dr F.C. Lovey and Dr A. Condó for the TEM experiments. Authors also want to acknowledge the financial support of Agencia Española de Cooperación Internacional (project A/8199/07), Spanish Ministerio de Ciencia e Innovación (EDARSOL project, CTQ 2009-13459-CO3-03), Universidad Politécnica de Valencia, and Agencia Nacional de Promoción Científica y Tecnológica (Argentina, project PICT 2008 # 0686). S.G.B., C.J.C. and M.C.G. are research members of CONICET, Argentina. D.O.M. is a research member of Comisión de Investigaciones Científicas de la Provincia de Buenos Aires (Argentina).

References

1 S. R. Shield and J. M. Harris, Reaction kinetics at dispersed-colloid/solution interfaces: benzophenone triplet-state quenching by methylated silica particles, *J. Phys. Chem. B*, 2000, **104**, 8527–8535.
2 V. B. Arce, S. G. Bertolotti, F. J. V. E. Oliveira, C. Airoldi, M. C. Gonzalez, P. E. Allegretti and D. O. Mártire, The use of molecular probes for the characterization of dispersions of functionalized silica nanoparticles, *Spectrochim. Acta, Part A*, 2009, **73**, 54–60.
3 A. E. Ruiz, P. Caregnato, V. B. Arce, M. M. Schiavoni, V. C. Mora, M. C. Gonzalez, P. E. Allegretti and D. O. Mártire, Synthesis and characterization of butoxylated silica nanoparticles. Reaction with benzophenone triplet states, *J. Phys. Chem. C*, 2007, **111**, 7623–7628.
4 V. B. Arce, S. G. Bertolotti, F. J. V. E. Oliveira, C. Airoldi, M. C. Gonzalez, P. E. Allegretti and D. O. Mártire, Safranine-T triplet-state quenching by modified silica nanoparticles, *J. Phys. Chem. C*, 2011, **115**, 18122–18130.
5 G. C. Ossenkamp, T. Kemmitt and J. H. Johnston, Toward functionalized surfaces through surface esterification of silica, *Langmuir*, 2002, **18**, 5749–5754.
6 G. C. Ossenkamp, T. Kemmitt and J. H. Johnston, New approaches to surface-alkoxylated silica with increased hydrolytic stability, *Chem. Mater.*, 2001, **13**, 3975–3980.
7 K. Van Hoecke, K. A. C. De Schamphelaere, P. Van der Meeren, S. Lucas and C. R. Janssen, Ecotoxicity of silica nanoparticles to the green alga *Pseudokirchneriella subcapitata*: importance of surface area, *Environ. Toxicol. Chem.*, 2008, **27**, 1948–1957.
8 V. B. Arce, J. A. Rosso, F. J. V. E. Oliveira, C. Airoldi, D. B. Soria, M. C. Gonzalez, P. E. Allegretti and D. O. Mártire, Generation of chemisorbed benzyl radicals on silica nanoparticles, *Photochem. Photobiol.*, 2010, **86**, 1208–1214.
9 S. Nonell, M. Gonzalez and F. R. Trull, I*H*-Phenalen-l-one-2-sulfonic acid: an extremely efficient singlet molecular oxygen sensitizer for aqueous media, *Afinidad*, 1993, **50**, 445–450.
10 S. Brunauer, P. H. Emmett and E. Teller, Adsorption of gases in multimolecular layers, *J. Am. Chem. Soc.*, 1938, 60, 309–319.
11 S. Parvez, C. Venkataraman and S. Mukherji, A review on advantages on implementing inhibition test (*Vibrio fischeri*) for acute toxicity prediction of chemicals, *Environ. Int.*, 2006, **32**, 265–268.
12 M. Gutierrez, J. Etxebarria and L. de las Fuentes, Evaluation of wastewater toxicity: comparative study between Microtox® and activated sludge oxygen uptake inhibition, *Water Res.*, 2002, **36**, 919–924.
13 G. Ricco, M. C. Tomei, R. Ramadori and G. Laera, Toxicity assessment of common xenobiotic compounds on municipal activated sludge: comparison between respirometry and Microtox®, *Water Res.*, 2004, **38**, 2103–2110.
14 S. Criado, S. G. Bertolotti, A. T. Soltermann and N. A. García, Kinetics studies on the photosensitized oxidation ($O_2(^1\Delta_g)$-mediated) of tryptophan-alkyl esters in Triton X-100 micellar solutions, *J. Photochem. Photobiol., B*, 1997, **38**, 107–113.
15 P. M. David Gara, G. N. Bosio, V. B. Arce, L. Poulsen, P. R. Ogilby, R. Giudici, M. C. Gonzalez and D. O. Mártire, Photoinduceddegradation of the herbicide clomazone. Model reactions for natural and technical systems, *Photochem. Photobiol.*, 2009, **85**, 686–692.
16 D. O. Mártire, P. Vaveliuk and G. Bilmes, Photophysical properties of corrphycenes, *Spectrochim. Acta, Part A*, 2000, **56**, 2043–2048.
17 H. L. Schmider and A. D. Becke, Optimized density functionals from the extended G2 test set, *J. Chem. Phys.*, 1998, **108**, 9624–9631.
18 V. Barone and M. Cossi, Quantum calculation of molecular energies and energy gradients in solution by a conductor solvent model, *J. Phys. Chem. A*, 1998, **102**, 1995–2001.
19 C. J. Cobos and A. E. Croce, Theoretical study of the absorption spectrum and the thermochemistry of the CF3OSO3 radical, *Z. Naturforsch.*, 2010, **65a**, 720–725.
20 Gaussian 09, Revision A.02, M. J. Frisch, G. W. Trucks, H. B. Schlegel, G. E. Scuseria, M. A. Robb, J. R. Cheeseman, G. Scalmani, V. Barone, B. Mennucci, G. A. Petersson, H. Nakatsuji, M. Caricato, X. Li, H. P. Hratchian, A. F. Izmaylov, J. Bloino, G. Zheng, J. L. Sonnenberg, M. Hada, M. Ehara, K. Toyota, R. Fukuda, J. Hasegawa, M. Ishida, T. Nakajima, Y. Honda, O. Kitao, H. Nakai, T. Vreven, J. A. Montgomery Jr., J. E. Peralta, F. Ogliaro, M. Bearpark, J. J. Heyd, E. Brothers, K. N. Kudin, V. N. Staroverov, R. Kobayashi, J. Normand, K. Raghavachari, A. Rendell, J. C. Burant, S. S. Iyengar, J. Tomasi, M. Cossi, N. Rega, J. M. Millam, M. Klene, J. E. Knox, J. B. Cross, V. Bakken, C. Adamo, J. Jaramillo, R. Gomperts, R. E. Stratmann, O. Yazyev, A. J. Austin, R. Cammi, C. Pomelli, J. W. Ochterski, R. L. Martin, K. Morokuma, V. G. Zakrzewski, G. A. Voth, P. Salvador, J. J. Dannenberg, S. Dapprich, A. D. Daniels, O. Farkas, J. B. Foresman, J. V. Ortiz, J. Cioslowski and D. J. Fox, Gaussian, Inc., Wallingford CT, 2009.
21 J. A. A. Sales, G. C. Petrucelli, F. J. V. E. Oliveira and C. Airoldi, Mesoporous silica originating from a gaseous ammonia epoxide ring opening and the thermodynamic data on some divalent cation adsorptions, *J. Colloid Interface Sci.*, 2007, **315**, 426–433.
22 J. A. A. Sales and C. Airoldi, Calorimetric investigation of metal ion adsorption on 3-glycidoxypropyltrimethylsiloxane + propane-1,3-diamine immobilized on silica gel, *Thermochim. Acta*, 2005, **427**, 77–83.
23 P. K. Jal, S. Patel and B. K. Mishra, Chemical modification of silica surface by immobilization of functional groups for extractive concentration of metal ions, *Talanta*, 2004, **62**, 1005–1028.
24 A. Jitianu, A. Crisan, A. Meghea, I. Raub and M. J. Zaharescua, Influence of the silica based matrix on the formation of iron oxide nanoparticles in the Fe_2O_3–SiO_2 system, obtained by sol–gel method, *J. Mater. Chem.*, 2002, **12**, 1401–1407.
25 G. E. Fryxell, Y. Lin, S. Fiskum, J. C. Birnbaum, H. Wu, K. Kemner and S. Kelly, Actinide sequestration using self-assembled monolayers on mesoporous supports, *Environ. Sci. Technol.*, 2005, **39**, 1324–1331.
26 A. Makkuni, R. S. Varma, S. K. Sikdar and D. Bhattacharyya, Aqueous and vapor phase mercury sorption by inorganic oxide materials functionalized with thiols and poly-thiols, *Clean Technol. Environ. Policy*, 2005, **7**, 87–96.
27 A. L. P. Silva, K. S. Sousa, A. F. S. Germano, V. V. Oliveira, J. G. P. Espínola, M. G. Fonseca, C. Airoldi, T. Arakaki and L. N. H. Arakaki, A new organofunctionalized silica containing thioglycolic acid incorporated for divalent cations removal – a thermodynamic cation/ basic center interaction, *Colloids Surf., A*, 2009, **332**, 144–149.
28 H. K. Kammler, G. Beaucage, R. Muellerand and S. E. Pratsinis, Structure of flame-made silica nanoparticles by ultra-small-angle x-ray scattering, *Langmuir*, 2004, **20**, 1915–1921.

29 L. T. Zhuralev, The surface chemistry of morphoussilica, Zhuravlev model, *Colloids Surf., A*, 2000, **173**, 1–38.
30 R. F. de Farias and C. Airoldi, Thermogravimetry as a reliable tool to estimate the density of silanols on a silica gel surface, *J. Therm. Anal. Calorim.*, 1998, **53**, 751–756.
31 J. Yang, J. Duan, D. Fornasiero and J. Ralston, Very small bubble formation at the solid–water interface, *J. Phys. Chem. B*, 2003, **107**, 6139–6147.
32 J. Yang, J. Duan, D. Fornasiero and J. Ralston, Kinetics of CO_2 nanobubble formation at the solid/water interface, *Phys. Chem. Chem. Phys.*, 2007, **9**, 6327–6332.
33 Z. Martinez-Ramirez, S. A. Jimenez-Lam and J. C. Fierro-Gonzalez, Infrared spectroscopic evidence of adsorbed species during the oxidation of 2-propanol catalyzed by γ-Al_2O_3-supported gold: Role of gold as a hydrogen-subtractor, *J. Mol. Catal. A: Chem.*, 2011, **344**, 47–52.
34 M. J. Llansola Portolés, F. Rodríguez Nieto, D. B. Soria, J. I. Amalvy, P. J. Peruzzo, D. O. Mártire, M. O. Kotler, O. Holub and M. C. Gonzalez, Photophysical properties of blue-emitting silicon nanoparticles, *J. Phys. Chem. C*, 2009, **113**, 13694–13702.
35 A. García, R. Espinosa, L. Delgado, E. Casals, E. González, V. Puntes, C. Barata, X. Font and A. Sánchez, Acutetoxicity of cerium oxide, titanium oxide and iron oxide nanoparticles using standardized tests, *Desalination*, 2011, **269**, 136–141.
36 K. Vaajasaari, M. Kulovaara, A. Joutti, E. Schultz and K. Soljamo, Hazardous properties of paint residues from the furniture industry, *J. Hazard. Mater.*, 2004, **106A**, 71–79.
37 B. Fubini, I. Fenoglio, M. Tomatis and F. Turci, Effect of chemical composition and state of the surface on the toxic response to high aspect ratio nanomaterials, *Nanomedicine*, 2011, **6**, 899–920.
38 M. B. Salerno, B. E. Logan and D. Velegol, Importance of molecular details in predicting bacterial adhesion to hydrophobic surfaces, *Langmuir*, 2004, **20**, 10625–10629.
39 J. Reynisson and S. Steenken, Hydrogen bonding between histidine and lignin model compounds or redox mediators as calculated with the DFT method. Effects on the ease of oxidation, *Org. Biomol. Chem.*, 2004, **2**, 578–584.
40 G. L. Hug, *Optical Spectra of Nonmetallic Inorganic Transient Species in Aqueous Solution*. National Standard Reference Data System, National Bureau of Standards Washington, Washington D. C., 1981, p6.
41 E. Baciocchi, M. Bietti, G. Ercolani and S. Steenken, OH-Induced shift from carbon to oxygen acidity in the side-chain deprotonation of 2-, 3- and 4-methoxybenzyl alcohol radical cations in aqueous solution: results from pulse radiolysis and DFT calculations, *Tetrahedron*, 2003, **59**, 613–618.
42 D. V. Avila, K. U. Ingold, A. A. Di Nardo, F. Zerbetto, M. Z. Zgierski and J. Lusztyk, Electronic absorption spectra of some alkoxyl radicals. An experimental and theoretical study, *J. Am. Chem. Soc.*, 1995, **117**, 2711–2718.
43 Y. Zhao and D. G. Truhlar, Density functionals with broad applicability in chemistry, *Acc. Chem. Res.*, 2008, **41**, 157–167.
44 K. Tokumura, T. Ozaki, H. Nosaka, Y. Saigusa and M. Itoh, Excited-state and ground-state reactivities of *para*-substituted benzyl radicals toward molecular oxygen, *J. Am. Chem. Soc.*, 1991, **113**, 4974–4980.
45 R. F. Weiss, Solubility of nitrogen,oxygen, and argon in water and sea water, *Deep-Sea Res. Oceanogr. Abstr.*, 1970, **17**, 721–735.
46 J. M. Achord and C. L. Hussey, Determination of dissolved oxygen in nonaqueous electrochemical solvents, *Anal. Chem.*, 1980, **52**, 601–602.
47 M. Koizumi, S. Kato, N. Mataga, T. Matsuura and I. Isui, *Photosensitized Reactions*. Kagakudogin Publishing Co, Kyoto, Japan, 1978.
48 M. Kasha, in: *Singlet O2*, ed. A. A. Frimer, CRC Press, Boca Raton, 1988; Vol. I, pp. 1–12.
49 C. Martí, O. Jürgens, O. Cuenca, M. Casals and S. Nonell, Aromatic ketones as standards for singlet molecular oxygen $O_2(^1\Delta_g)$ photosensitization. Time-resolved photoacoustic and near-IR emission studies, *J. Photochem. Photobiol., A*, 1996, **97**, 11–18.
50 F. Wilkinson, W. P. Helman and A. B. Ross, Rate constants for the decay and reactions of the lowest electronically excited singlet state of molecular oxygen in solution. An expanded and revised compilation, *J. Phys. Chem. Ref. Data*, 1995, **24**, 663–678.

